

Numerical Analysis of Laser Induced Photothermal Effects using Colloidal Plasmonic Nanostructures

Ioannis H. Karamelas¹, Young Hwa Kim² and Edward P. Furlani^{1,2}

¹ Dept. of Chemical and Biological Engineering, ² Dept. of Electrical Engineering,
University at Buffalo SUNY, NY 14260, Office: (716) 645-1194, Fax: (716) 645-3822, efurlani@buffalo.edu

ABSTRACT

Colloidal noble metal (plasmonic) nanostructures are finding increasing use in a variety of photothermal applications that range from nanoparticle synthesis to bioimaging to medical therapy. In many applications, a pulsed laser is used to excite the plasmonic nanostructures at their plasmon resonant frequency, which results in a peak absorption of incident photons and highly localized (sub-wavelength) field enhancement. In addition to enabling efficient nanoscale heating from a remote source, the resonant heating wavelength can be tuned within the ultraviolet through near-infrared spectrum by adjusting the geometry of the nanoparticle during synthesis. Following our previous work [1, 2], we present computational models to predict various photonic and thermo-fluidic aspects associated with nanosecond-pulsed, laser-heated colloidal metallic nanoparticles. We simulate energy conversion within different nanoparticle structures at plasmon resonance, heat transfer from the particle to the surrounding fluid and phase change of the fluid leading to homogenous bubble nucleation. We consider various nanoparticle geometries including nanorods, nanotori, nanorings and nanocages. We show that various process parameters such as the laser intensity, incident wavelength, polarization, pulse duration and the orientation and shape of the nanoparticles can be tuned to optimize the photothermal process. We discuss the utilization of such nanoparticles in photothermal applications involving bioimaging, drug delivery and therapy of malignant tumors.

Keywords: Localized surface plasmon resonance (LSPR), photothermal energy conversion, plasmonic-enhanced photothermal energy transfer, LSPR-induced optical absorption, pulsed-laser photothermal heating.

1 INTRODUCTION

The ability to control thermal energy at the nanoscale is finding increasing use in emerging applications in fields such as nanoparticle synthesis, imaging and medical therapy, among others [3, 4]. Laser-based plasmon-enhanced photothermal energy conversion is of particular interest as it enables efficient heating with unprecedented (subwavelength) spatial resolution. In this approach, a pulsed laser is used to heat metallic nanostructures at their plasmon

resonance frequency, which can be tuned from ultraviolet through the near-infrared spectrum using different shaped particles [1, 5]. The plasmon resonance and associated absorption spectrum are well investigated analytically and numerically for several nanoparticle geometries including nanospheres, nanorods, and nanoshells [6-12]. However, fewer results exist for nanotorus, nanoring and nanocage structures. In this presentation we use computational models to investigate the plasmon resonance behavior of these geometries, especially their absorption spectrum at different orientations with respect to the incident polarization. We present, for the first time, the plasmonic response and thermofluidic behavior of laser-pulsed colloidal gold nanocage structures. For all cases studied, we consider nanosecond-pulsed laser illumination of the nanoparticles in fluid leading to bubble nucleation, wherein the pulse duration exceeds the characteristic time constants for initial non-equilibrium photothermal transient effects. Our results show that randomly oriented nanotorus and nanoring particles are best suited for colloidal photothermal manifestation due to their high absorption efficiency. We also demonstrate that nanocages exhibit a resonance peak in the NIR which makes them exceptionally effective for deep tumor penetration and photothermal drug delivery.

2 RESULTS AND DISCUSSION

We model laser-induced plasmon-assisted photothermal effects using continuum level photonic and fluidic analysis. The photonic analysis is performed using computational electromagnetics and is used to predict photothermal energy conversion within the nanoparticles, i.e. the time-averaged power absorbed by a particle as a function of the wavelength and polarization of the incident light. Maximum power absorption occurs at the plasmon resonant wavelength, which depends on the size, geometry and optical properties of the particle. The absorbed power is converted into heat and thus the particle becomes a heat source within the fluid. As the particle heats up, thermal energy is transferred to the fluid and a vapor bubble will nucleate at the particle-fluid interface if the critical vaporization temperature of the fluid is reached. Once nucleated, a bubble will exhibit a dynamic behavior (expansion and collapse) that is a complex function of the heat and mass transfer at the bubble-fluid interface as well as the temperature and flow in the surrounding fluid. This is simulated using computational fluid dynamic (CFD) analysis.

2.1 PHOTONIC SIMULATIONS

For the photonic analysis we use 3D full-wave time-harmonic field theory. We perform the numerical simulations using the finite element-based COMSOL RF solver (www.comsol.com). The computational domain for the nanotorus geometry is shown in **Fig.1a** [1].

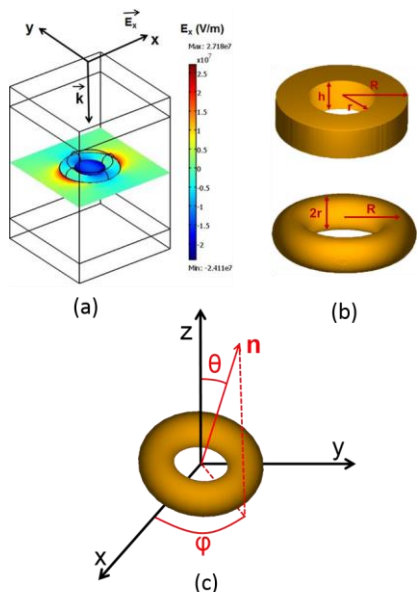


Figure 1. Photonic analysis, particle geometries and orientations: (a) computational domain and field analysis for a nanotorus, (b) nanoring (top) and nanotorus (bottom) geometries, (c) nanotorus and nanoring orientations [1, 2]

The torus is located at the origin of the computational domain and the incident field is generated by a surface current (not shown) in the xy -plane at the top of the computational domain, which results in a TEM plane wave with the electric field polarized in the x -direction and the wave propagating downwards along the z -axis as indicated by the \mathbf{k} vector. The permittivity of gold nanoparticles is

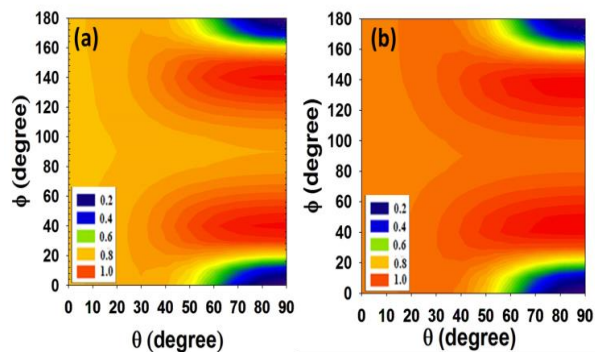


Figure 2. NIR absorption at a fixed LSPR wavelength as a function of orientation (θ and ϕ): (a) nanoring at $\lambda=793\text{nm}$ ($r=20\text{nm}$, $R=40\text{nm}$), (b) nanotorus at $\lambda=825\text{nm}$ ($r=10\text{nm}$, $R=30\text{nm}$).

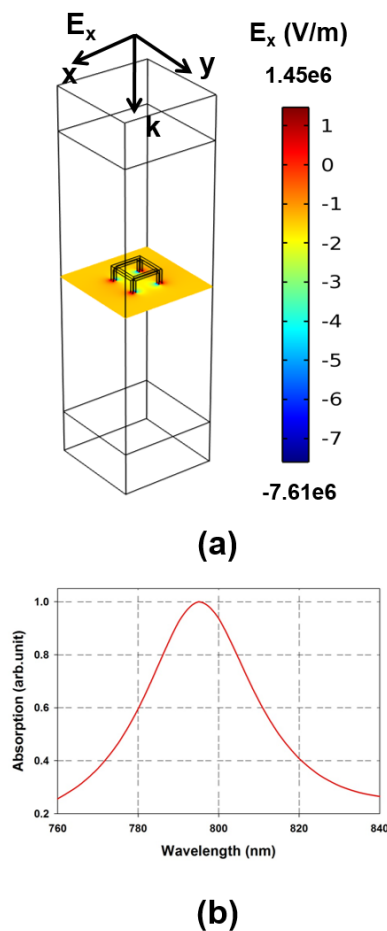


Figure 3. Photonic analysis of a gold nanocage ($a=50\text{nm}$ and $t=5\text{nm}$) with parallel alignment to the incident polarization: (a) Computational domain and plot of E_x through a cross section of the domain, (b) absorbed power vs. wavelength at parallel orientation.

predicted using an analytical expression that is based on a Drude-Lorentz model as described in our previous work [1, 2]. The parameters for this equation can be found in the literature [13-15]. It is instructive to investigate the plasmon resonance of nanotori and nanorings and compare absorption spectra, at different orientations relative to the incident polarization (**Fig. 1b, c**). We set the torus minor radius to $r=10\text{nm}$ and its major radius to $R=30\text{nm}$. The inner and outer radii (r, R) for the nanoring are 20nm and 40nm respectively and its height is $h=20\text{nm}$.

As shown in **Fig. 2**, the absorption spectra vs. orientation of the nanoring is essentially the same as that of the nanotorus. In both cases high absorption is achieved throughout a wide range of possible orientations. In fact, our results show that peak absorption occurs at orientations offset in an angular sense from parallel alignment with the incident field. Hence, we find that nanorings and nanotori can be essentially interchanged for photothermal applications. This is in contrast to the nanorod where, for

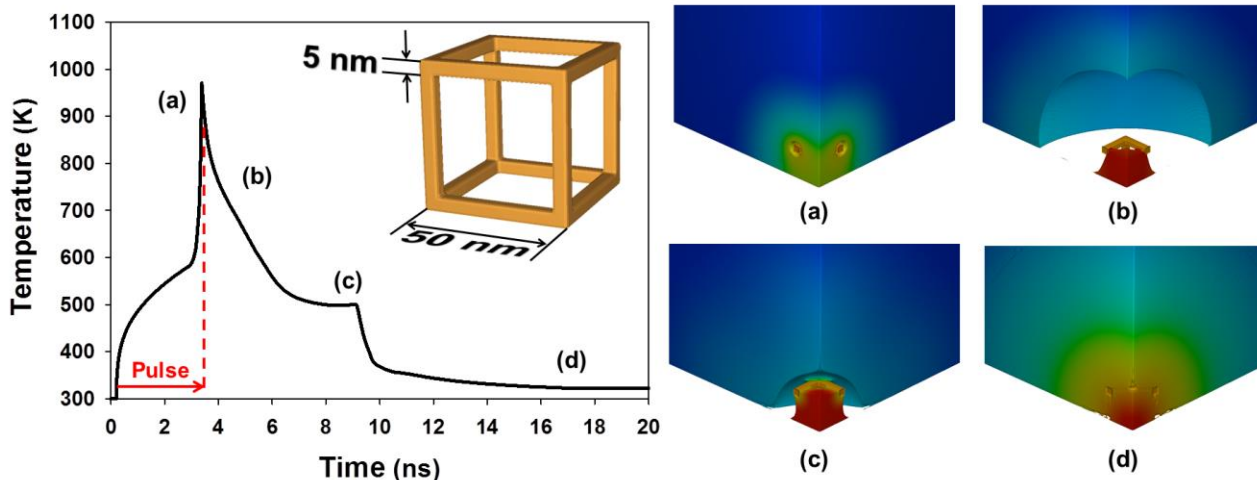


Figure 4. Photothermal heat cycle of a nanocage ($a=50\text{nm}$, $t=5\text{nm}$) (perspective 1/8 view): plot of nanocage temperature vs. time, pulse duration indicated by the red arrow and dashed line and inset plots showing various phases of the thermo-fluidic cycle: (a) nanobubble formation, (b) nanobubble (maximum size), (c) nanobubble collapse, (d) cooling.

NIR resonance, high absorption is restricted to (near) parallel polarized orientations [2].

Next, we consider the nanocage structure. Gold nanocages represent a more recent advance in the field of nanoparticle synthesis that is especially well suited for photothermal therapeutic applications [16]. One major advantage of this geometry is that it can be readily fabricated in large quantities using bottom-up techniques [17]. Another discriminating property of nanocages compared to other nanostructures is their porosity. Given their porous structure, gold nanocages can be discriminated from nanoparticles of similar size using nanocage-based biomarkers and analyzing transmission electron microscopy (TEM) images. Thanks to their porous properties, nanocages are uniquely suited for drug encapsulation and optically controlled photothermal drug delivery [18].

We study the behavior of a cubic nanocage with sides that are 5nm thick and 50nm in length. The nanocage is illuminated with a downward directed uniform TEM plane wave with \mathbf{E} parallel to the x-axis as shown in **Fig. 3a**. We performed a parametric analysis of the power absorbed by the nanocage as a function of wavelength for $\lambda = 760\text{-}840\text{ nm}$. Plasmon resonance was found to occur at 795 nm (**Fig. 3b**).

2.2 FLUIDIC SIMULATIONS

CFD analysis was performed to determine the power and pulse duration required to achieve bubble nucleation without melting the nanocage. A 3D CFD analysis was performed so as to determine the pulse duration and power required for the nucleation of a nanobubble without damaging or melting the nanostructure. It sufficed to model one octant of the nanocage due to its symmetry.

The analysis was divided into two phases. In the first phase, we predicted the power level required to heat the nanocage from an ambient temperature of 300K to the superheat temperature of the carrier fluid, i.e. 580K for water. This depends on the pulse duration, which was constrained to be between 3 to 5 ns. In the second phase of the analysis, we applied the power levels obtained in phase one and increased the pulse duration so that the nanoparticles were heated beyond the superheat temperature, which caused vaporization of the surrounding fluid and bubble nucleation. The pulse duration was tuned so that the nanoparticle achieved a temperature that was sufficiently high to generate a sustained nanobubble, but low enough ($< 1100\text{K}$) to avoid melting the nanoparticle. Based on our analysis, it was found that a power of $180\ \mu\text{W}$ with pulse duration of 3.18 ns is adequate for nucleation. The results of the thermo-fluidic analysis are shown in **Fig. 4**.

Initially, the nanocage and the fluid are at the ambient temperature 300K. The heat pulse starts after 0.2 ns causing a gradual rise in the temperature of the nanoparticle, which is indicated in the temperature vs. time plot of **Fig. 4**. This continues until the nanoparticle reaches the superheat temperature, at which point a homogeneous bubble is nucleated around it. Upon nucleation, a thin sheath of vapor surrounds the nanocage and insulates it. Since power is still being dissipated in the nanoparticle, its temperature rises rapidly. This continues until the end of the heat pulse, which coincides with the bubble formation and maximum temperature as shown in plot segment and inset figure (a). The pulse duration is 3.18 ns as indicated by the red dashed line. As soon as the nanobubble forms, it expands due to its high pressure relative to the surrounding fluid. The nanobubble reaches a maximum size as shown in inset figure (b). The maximum bubble radius achieved was 120 nm. Subsequently, the bubble contracts and collapses bringing

fluid back in contact with the nanoparticle as shown in plot segment and inset figure (c). The nanoparticle gradually cools to the ambient temperature as more of the fluid comes in contact with it as shown in plot segment and inset figure (d). An interesting observation of this process is the formation of a hot droplet of fluid in the middle of the nanoparticle, which partially evaporates as the nanobubble expands. The CFD simulation was performed on Hex-core workstation with 32 GB of RAM. The time for the simulation was approximately 12 days.

2.3 PHOTOTHERMAL CANCER THERAPY

Plasmonic nanoparticles are utilized for cancer therapy by delivering localized thermal energy to the tumor site when illuminated at plasmonic resonance [19]. Such localized field causes hyperthermia which leads to the death of tumor cells.

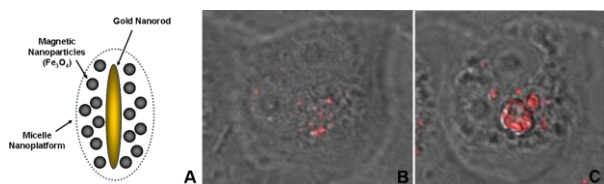


Figure 5. Photothermal Therapy: (a) Magneto-plasmonic nanoplatfom, (b, c) pre- and post- illumination images of HeLa cells, (c) Nanobubble nucleation generated by nanoplatfom when illuminated by a 780nm pulsed laser [20].

Recently, an approach for enhanced therapy has been reported that involves a combination of nanomagnetics (for field-directed targeting of tumor cells) and plasmonics for photothermal treatment. Phospholipid micelles were used to contain a gold nanorod along with (15-20) magnetite nanoparticles. This magneto-plasmonic nanoformulation can be manipulated using an external magnetic field for directed targeting of malignant tissue. Upon cellular uptake, the nanoplatfom was irradiated by a femtosecond-pulsed laser at a plasmon resonant wavelength (780nm) of the nanorod. The heated nanorod created nanobubbles that destroyed the cancer cells, as seen in **Fig. 5**. The combined functionality of the novel magneto-plasmonic structures produces a synergistic therapeutic effect that results in increased specificity and efficacy of photothermal cancer treatment, while reduced laser fluence holds promise for the treatment of deeper tumors [20].

3 CONCLUSIONS

We have used a combination of computational electromagnetic and fluid dynamic analysis to study nanosecond-pulsed laser heating of nanotorus, nanoring and nanocage structures. We have showed that nanotori and nanorings exhibit similar absorption behavior and compared to nanorods, they have a higher average absorption for random orientations when illuminated with the appropriate

plasmon resonance frequency. We have also investigated photothermal effects of nanocage structures and found that it holds promise for photothermal therapy as well. Our modeling approach can be used to explore fundamental behavior of nanoscale photothermal processes and is useful for the rational design of novel plasmonic structures for a wide range of applications.

REFERENCES

- [1] Furlani, E. P., Karampelas I. H., et al. (2012), Lab on a Chip **12**(19): 3707-3719
- [2] Alali, F., Karampelas, I.H., et al. (2013), Journal of Physical Chemistry C **117**: 20178-20185
- [3] West, J. L. and Halas N. J. (2000). Current Opinion in Biotechnology **11**(2): 215-217
- [4] Pitsillides, C.M., et al. (2003). Biophysics Journal. **84**: 4023-4032
- [5] Roper, D.K., Ahn W. et al. (2007). J. Phys. Chem. C **111**(9): 3636-3641
- [6] Dutta C. M. et al (2008), J. Phys. **129**, 084706
- [7] Ekici, O., Harrison R. K., et al. (2008) Journal of Physics D-Applied Physics. **41**.
- [8] Hao E., Schatz G. et al. (2004). J. Fluoresc., **14**: 331–341
- [9] Sonnichsen C., Franzl T., et al. (2002), Phys. Rev. Lett., **88**: 077402
- [10] Hao E. and Schatz G. (2004) J. Chem. Phys. **120**: 357–366
- [11] Hu M., Chen J., et al. (2006) Chem. Soc. Rev. **35**: 1084–1094
- [12] Brandl D. W. and Nordlander P. (2007), J. Chem. Phys. **126**: 144708
- [13] Jain P. K., Huang X. H., et al. (2008), Acc. Chem. Res. **41**: 1578–1586
- [14] Kreibitz U. and Vollmer M. (1995), Optical Properties of Metal Clusters, Springer, Berlin
- [15] Lewinski N., Colvin V., et al. (2008), Small. **4**: 26–49.
- [16] O'Neal, D.P. et al. Cancer Letters, 2004. **209**(2): 171-176.
- [17] Skrabalak, S.E., et al. (2008), Accounts of Chemical Research, **41**(12): 1587-1595
- [18] Khlebtsov, N., et al. (2013) Theranostics, **3**(3): 167-180
- [19] Huff T. B., Tong L., et al. (2007), Nanomedicine **2**(1): 125–132
- [20] Ohulchanskyy T.Y., Kopwiththaya A., et al. (2013) Nanomedicine **9**:1192-1202